Acta Pharmaceutica Sinica B 2024;14(7):2959–2976

Chinese Pharmaceutical Association
Institute of Materia Medica, Chinese Academy of Medical Sciences

Acta Pharmaceutica Sinica B

www.elsevier.com/locate/apsb
www.sciencedirect.com

ORIGINAL ARTICLE

KHK-A promotes fructose-dependent colorectal cancer liver metastasis by facilitating the phosphorylation and translocation of PKM2

Chaofan Peng[a,b,c,†], Peng Yang[a,b,c,†], Dongsheng Zhang[a,b,c,†], Chi Jin[a,b,c,†], Wen Peng[a,b,c], Tuo Wang[a,b,c], Qingyang Sun[a,b,c], Zhihao Chen[a,b,c], Yifei Feng[a,b,c,d,*], Yueming Sun[a,b,c,d,*]

[a]*Department of General Surgery, the First Affiliated Hospital of Nanjing Medical University, Nanjing 210029, China*
[b]*Colorectal Institute of Nanjing Medical University, Nanjing 210029, China*
[c]*The First School of Clinical Medicine, Nanjing Medical University, Nanjing 210029, China*
[d]*Jiangsu Province Engineering Research Center of Colorectal Cancer Precision Medicine and Translational Medicine, Nanjing 210029, China*

Received 13 January 2024; received in revised form 1 March 2024; accepted 15 April 2024

KEY WORDS

CRC;
CRLM;
Fructose;
KHK-A;
PKM2

Abstract Excessive fructose diet is closely associated with colorectal cancer (CRC) progression. Nevertheless, fructose's specific function and precise mechanism in colorectal cancer liver metastasis (CRLM) is rarely known. Here, this study reported that the fructose absorbed by primary colorectal cancer could accelerate CRLM, and the expression of KHK-A, not KHK-C, in liver metastasis was higher than in paired primary tumors. Furthermore, KHK-A facilitated fructose-dependent CRLM *in vitro* and *in vivo* by phosphorylating PKM2 at Ser37. PKM2 phosphorylated by KHK-A inhibited its tetramer formation and pyruvic acid kinase activity but promoted the nuclear accumulation of PKM2. EMT and aerobic glycolysis activated by nuclear PKM2 enhance CRC cells' migration ability and anoikis resistance during CRLM progression. TEPP-46 treatment, targeting the phosphorylation of PKM2, inhibited the pro-metastatic effect of KHK-A. Besides, c-myc activated by nuclear PKM2 promotes alternative splicing of KHK-A, forming a positive feedback loop.

*Corresponding authors.
E-mail addresses: sunyueming@njmu.edu.cn (Yueming Sun), fengyifei1982@163.com (Yifei Feng).
[†]These authors made equal contributions to this work.
Peer review under the responsibility of Chinese Pharmaceutical Association and Institute of Materia Medica, Chinese Academy of Medical Sciences.

https://doi.org/10.1016/j.apsb.2024.04.024

1. Introduction

Colorectal cancer (CRC) is the second most deadly cancer[1]. Colorectal cancer liver metastasis (CRLM) is the leading cause of its low survival rate[2,3]. Due to the portal vein circulation and rich blood supply, the liver is the most common metastatic organ of CRC. Up to 30%−50% of CRC patients suffer from CRLM during the disease process[4]. Though comprehensive therapy, including surgical excision, locoregional metastases ablation, chemotherapy and immunotherapy, has been extensively applied in CRLM treatment, the long-term survival rate of CRLM patients remains poor. Therefore, exploring the potential mechanism and developing therapeutic targets is urgent.

Notably, the incidence of early-onset colorectal cancer (CRC patients diagnosed at younger than 50 years old) has been on the rise, and early-onset colorectal cancer patients had more synchronous metastatic presentation than screening-age colorectal cancer patients over decades[5,6]. Increased high-fructose corn syrup in the young population is one of the critical risk factors[5]. Fructose tastes much sweeter than other hexoses, but its metabolic mechanism is distinct from glucose in several ways[7]. In addition, fructose is closely related to multiple cancer progression, including breast, pancreatic and colorectal cancer[8-10]. Colorectal cancer cells undergo metabolic reprogramming after colonization in the liver, and the upregulation of aldolase B (ALDOB) enhances fructose metabolism and provides carbon source for tumor cell proliferation[10]. Elevated GLUT5 promotes fructose utilization and CRC growth[11]. Various metabolic enzymes play crucial roles in cancer progression *via* metabolic and nonmetabolic avenues[12,13]. Ketohexokinase (KHK) is the first rate-limiting enzyme in fructose metabolism. The alternative splicing of exon 3 generates two distinct isoforms, KHK-A and KHK-C. KHK-C is mainly expressed in hepatocytes and can phosphorylate fructose to fructose-1-phosphate, while KHK-A is expressed in several cancer tissues and hardly phosphorylate fructose[7,14]. The role of KHK-A in CRLM is still unclear.

Cancer cells tend to drastically enhance glycolytic rates rather than promote the tricarboxylic acid cycle even in the presence of adequate oxygen supply, known as the Warburg effect, a hallmark of cancer[15]. PKM2 (pyruvate kinase M2) is the critical regulator of the Warburg effect. Impaired pyruvic acid kinase activity results in a metabolic shift to biosynthetic processes, and post-translational modifications of PKM2 alter its PK activity differentially[16]. The phosphorylation of PKM2 at Ser37 is proposed to promote the nuclear translocation of PKM2 and the Warburg effect[17].

This report elucidates that fructose absorbed by primary colorectal cancer tissues promotes CRLM. KHK-A is upregulated in liver metastases compared to primary tumors. Furthermore, KHK-A accelerates fructose-dependent CRLM by promoting the epithelial−mesenchymal transition and aerobic glycolysis. The Warburg effect activated by KHK-A assists colorectal cancer cells in overcoming anoikis during metastatic progression and finally results in liver metastasis formation. Mechanically, fructose causes the interaction between KHK-A and PKM2. KHK-A phosphorylates PKM2 at Ser37, promotes its nuclear translocation and impairs the enzymatic activity of PKM2 under fructose stimulation. Besides, c-myc upregulated by nuclear PKM2 promotes alternative splicing of KHK-A, forming a positive feedback loop.

2. Materials and methods

2.1. Clinical specimens and cell culture

All paired primary colorectal cancer and liver metastatic tissues were obtained from patients who accepted synchronous surgery for CRLM at The First Affiliated Hospital of Nanjing Medical University (Nanjing, China). Fresh tissues were collected for metabolite detection, qRT-PCR and WB. A formalin-fixed paraffin-embedded tissue microarray of 48 paired primary and metastatic tumors was constructed by Servicebio (Wuhan, China). The major clinical information of these patients is listed in Supporting Information Table S1. The Human Ethics Committee approved this study.

Human DLD-1 and SW-480 cell lines were purchased from the Cell Bank of Type Culture Collection of the Chinese Academy of Sciences (Shanghai, China) and cultured in RPMI 1640 and L-15 medium, respectively, with 10% fetal bovine serum (FBS). 5 mmol/L fructose was used for fructose treatment cells.

2.2. Fructose concentration analysis

The fructose concentration of mice colorectal tissues was detected by a Fructose Assay Kit (Millipore Sigma, USA) according to the manufacturer's protocol. Mice tissues were homogenized in the Fructose Assay Buffer, and the Master Reaction Mix was added to each sample. The concentration of fructose was measured by colorimetric assay.

Fresh colorectal tissue slices were placed in 24-well plates containing glucose-free DMEM with 10% FBS and 5 mmol/L fructose. Then, the samples were cultured at 37 °C and 5% CO_2 for 72 h. The remaining fructose of related media was detected using the Fructose Assay Kit. The Fructose Assay Buffer and the Master Reaction Mix were added to each sample successively. The remaining fructose of the samples was detected by colorimetric detection after incubation for 2 h at 37 °C. Fructose uptake was calculated by subtracting the remaining fructose from the total fructose.

2.3. RNA extraction and qRT-PCR

Total RNA of tissues and cell lines was extracted with TRIzol reagent (Invitrogen, USA) according to the manufacturer's instructions. The quality and quantity of total RNA was measured using NanoDrop. Total RNA was reverse transcribed to cDNA using the RT Mix (Vazyme, China). A Sybr green kit (TaKaRa Biotechnology, China) was used for qRT-PCR with relative primers by Applied Biosystems 7500 Sequence Detection System.

The primer sequences are shown in Supporting Information Table S2.

2.4. Western blot and immunohistochemistry

We used a RIPA kit (Beyotime, China) supplemented with phenylmethanesulfonyl fluoride to extract cell or tissue protein lysate according to the protocols. The protein concentration of related samples was measured by the BCA Protein Assay Kit (Beyotime). After the protein lysate was separated on SDS-PAGE (Beyotime), it was transferred to a polyvinylidene fluoride membrane (Millipore, USA). The related membranes were blocked by QuickBlock (Beyotime) for 30 min and incubated with the primary antibody at 4 °C overnight. After the membranes were incubated with the secondary antibody for 2 h, the blots were obtained by exposure. Immunohistochemistry (IHC) of tissues was performed as previously described[18]. The antibodies used in this study are listed in Supporting Information Table S3.

2.5. Transwell assay

Cells with corresponding treatment resuspended in serum-free medium were seeded into the upper chamber of the transwell membrane (Millipore Sigma, USA). After 24 h (or 48 h based on cell types), cells adhering to the underside of the membrane were stained with crystal violet. Stained cells were counted under the microscope.

2.6. Co-IP and GST pull-down

The co-IP (co-immunoprecipitation) kit was performed with the IP/co-IP kit (Thermo Fisher Scientific) according to the manufacturer's protocol. Cell lysate was obtained by IP Lysis Buffer and incubated with the primary antibody at 4 °C overnight. Then, the magnetic beads were incubated with the immune complex for 1 h. After the magnetic beads were washed three times, the immunoprecipitates were supplemented with 1× SDS loading buffer and analyzed by WB or mass spectrometry.

GST-KHK-A, GST-KHK-A L73A and GST-KHK-A G257R were expressed and purified as described previously[14]. Glutathione agarose beads were incubated with purified protein for 12 h. Interacted protein was eluted with elution buffer after washed three times. Protein lysate obtained by GST Pull-down was separated on SDS-PAGE and analyzed by Coomassie Brilliant Blue (Beyotime) staining or WB.

2.7. Immunofluorescence

An Immunol Fluorence Staining Kit (Beyotime) was used for Immunofluorescence (IF). Firstly, cells planted in a confocal dish were fixed with the fixative solution. Then, we used the scrub solution to wash cells three times. Then, we incubated cells with relative primary antibody at 4 °C overnight after blocking buffer incubation. Finally, cells were incubated with the secondary antibody for 1 h, and the cell nucleus was stained with the DAPI (4′,6-diamidino-2′-phenylindole) staining solution. The results were analyzed using the confocal fluorescence microscopy.

2.8. In vitro kinase assay

Purified recombinant GST-KHK-A, His-PKM2 and their mutants were incubated in kinase buffer and 5 mmol/L fructose at 37 °C for 1 h. The reaction was then terminated by boiling with SDS-PAGE loading buffer for 10 min. The results were analyzed by WB.

2.9. Subcellular fractions isolation of protein

The isolation of subcellular fractions of protein was performed by nuclear and cytoplasmic extraction reagents (Thermo Fisher Scientific) according to the manufacturer's protocol. The Cytoplasmic Extraction Reagent was incubated with harvested cells and centrifuged for 5 min. Then, we transfer the supernatant (cytoplasmic extract) to a new tube. The insoluble fraction was suspended in the ice-cold Nuclear Extraction Reagent. The samples were vortexed and centrifuged. The supernatant was transferred to a new tube (nuclear extract). The subcellular fraction isolation of protein was analyzed by WB. Lamin-B1 and β-actin were used for nuclear and cytoplasmic loading controls.

2.10. Chromatin immunoprecipitation

A Chromatin Immunoprecipitation (ChIP) Kit (Cell Signaling Technology) was used for the ChIP assay. The assay was performed as previously reported[19]. Cells were incubated with glycine solution for 5 min after being crosslinked in 1% formaldehyde for 10 min. Then, the crosslinked cells were cracked with ChIP sonication cell lysis buffer. 90% chromatin was sheared to fragments concentrated between 200 and 1000 bp. The sheared chromatin fragments were incubated with beads and antibodies. The results were analyzed using qRT-PCR. The primer sequences are shown in Table S2.

2.11. Flow cytometry assay of anoikis

Cells were harvested after being cultured in low attachment plates for 72 h. The anoikis ratio was measured by Annexin V-APC/7-AAD Apoptosis Kit (Multi Sciences, Hangzhou, China). Cells were harvested and resuspended in the binding buffer. 5 μL Annexin V-APC and 10 μL 7-AAD were added to each tube. The apoptotic rates were analyzed using CytoFLEX S (Beckman Coulter, USA).

2.12. Pyruvate kinase activity assay and lactate detection assay

Pyruvate kinase activity was detected with a Pyruvate Kinase Activity Assay Kit (Thermo Fisher Scientific). Briefly, cells or tissues were rapidly homogenized in Pyruvate Kinase Assay Buffer, and colorimetric detection was used to qualify pyruvate kinase activity. The protein concentration of related samples was measured by the BCA Protein Assay Kit. PK activity was normalized to protein concentration.

The lactate concentration was measured using a Lactate Assay Kit (Thermo Fisher Scientific). Cells and tissues were rapidly homogenized in Lactate Assay Buffer, and colorimetric detection was used to quantify the lactate concentration. The protein concentration of related samples was measured by the BCA Protein Assay Kit. Lactate concentration was normalized to protein concentration.

2.13. Extracellular acidification rate

The Seahorse XFE (Agilent) was used to explore cells' ECAR (the extracellular acidification rate) according to the manufacturer's

protocol. Glucose, Oligomycin and 2-DG were added to each well in turn. The basic glycolysis and glycolytic capacity levels of related cells were analyzed.

2.14. Organoids construction

Primary and metastatic organoids were constructed as previously reported[20]. Fresh primary and liver metastatic colorectal cancer tissues were obtained after surgery. Tissues were washed using ice-cold PBS with penicillin and streptomycin 5 times. Each sample was cut into pieces and then digested in the digestion medium for 30 min at 37 °C. Digested cells were obtained through 100 μm cell filters and embedded in Matrigel on a well of 24-well cell culture plate. Human Colorectal Cancer Organoid Culture Medium (Absin, China) was used for organoid culture.

2.15. Animal models

The CRLM mice model was constructed as previously reported[21]. Firstly, the AOM/DSS model was constructed. C57BL/6J male mice were intraperitoneally injected with azoxymethane (AOM, Sigma) (10 mg per kg body weight) at 8 weeks old. Seven days later, the mice were treated with 2.5% dextran sulfate sodium (DSS, MP Biologicals) drinking water for 1 week and normal drinking water for 2 weeks. This schedule was repeated for 3 cycles. Additionally, 15% fructose water for 2 weeks after 3 cycles was aimed to measure the fructose ingestion effect of colorectal tumor tissue. For the CRLM model, 1×10^6 MC38 cells were injected into the spleen tip of AOM/DSS model mice in the tenth week. Mice were sacrificed 3 weeks after injection, and the livers of mice were obtained. For the subcutaneous xenograft model, 1×10^6 DLD-1 cells with sh-KHK, rKHK-C and rKHK-A transfection were separately injected into the groins of BALB/c nude mice with or without 15% fructose drinking water after injection. The sizes of the tumors were measured every week. The mice were sacrificed, and the xenograft tumors were dissected three weeks after the injection. All the animal experiments were ratified by the Committee on the Ethics of Animal Experiments of Nanjing Medical University.

2.16. Statistics analysis

All statistical analyses were performed with GraphPad Prism 8.0 (La Jolla, USA). The student's *t*-test was performed to analyze the difference between the two samples, while ANOVA was used for tests among more than two groups. Pearson's correlation analysis was performed for the correlation analysis. The significance threshold of each test was set at 0.05.

3. Results

3.1. Fructose absorbed by colorectal cancer tissue could accelerate CRLM

To investigate the effect of fructose on colorectal cancer liver metastasis, we performed the transwell assay upon fructose stimulation. The results indicated that fructose could promote the invasive ability of CRC cells in a time-dependent manner (Supporting Information Fig. S1A). Moreover, fructose treatment could activate EMT (epithelial−mesenchymal transition) (Fig. S1B). We constructed the AOM/DSS model on C57BL/6J mice and added a fructose diet for 2 weeks after the routine feeding process (Fig. 1A and B, Fig. S1C). The fructose concentration in colorectal tissues indicated that the fructose concentration in colorectal tumors was higher than normal and inflammatory colorectal epithelial tissues (Fig. 1C). GLUT5, the major fructose transporter, was upregulated in colorectal tumors (Fig. 1D)[22]. A previous metabolomics dataset analysis between primary CRC and liver metastasis showed that dihydroxyacetone phosphate and fructose 1,6-bisphosphate, two representative fructose downstream metabolites, were significantly upregulated in liver metastases compared to the matched primary tumors (Fig. 1E)[10]. Furthermore, we detected the fructose uptake ability in 4 patients' tissues, including normal tissues, primary, and liver metastatic tumors. The fructose uptake rate of the primary tumors was higher than that of normal tissues, while the uptake rate of liver metastases was higher than that of primary tumors (Fig. 1F). To further explore if the fructose untaken by colorectal tumor could promote CRLM, 2,5-anhydro-D-mannitol (2,5-AM), an inhibitor of fructose translocator, was used for fructose uptake inhibition of tumor cells[23]. 2,5-AM treatment inhibited fructose-induced cell invasion (Fig. S1D).

Then, we aimed to explore whether fructose taken by cancer tissues could promote CRLM *in vivo*, meaning that a mouse model with both primary and metastatic tumors was indispensable. However, the frequency of liver metastases is extremely low in the AOM/DSS model[24]. So, we injected MC38 cells intrasplenically into the AOM/DSS model to mimic human CRLM progression as previously reported[21]. 2,5-AM was used to inhibit fructose uptake by tumor cells (Fig. 1G). The high fructose diet could enhance CRLM and decrease the survival rate of mice, while 2,5-AM could impair the metastatic effect of the high fructose diet (Fig. 1H). The fructose concentration of liver metastases was higher than the primary tumor of the CRLM model with 15% fructose drinking water (Fig. S1E). The above findings elucidated that fructose absorbed by colorectal cancer cells could be used to accelerate CRLM progression.

3.2. KHK-A, rather than KHK-C, was significantly upregulated in liver metastasis

Emerging evidence demonstrated that metabolic enzymes could participate in tumor progression through metabolic and non-metabolic paths[12,13]. We analyzed the expression of fructose metabolism enzyme in 3 matched primary colorectal cancer and liver metastatic tissues *via* RNA-seq and proteomic. KHK, the first rate-limiting enzyme in fructose metabolism, was significantly upregulated in liver metastases (Fig. 2A and B). Furthermore, the expression of KHK in colorectal cancer liver metastases was higher than in primary tumors, according to GSE41528 (Fig. 2C). KHK expression in 8 matched PT and LM tissues was detected through qRT-PCR (Fig. 2D). KHK owns two distinct isoforms, KHK-A and KHK-C, through the splicing of exon 3 (Supporting Information Fig. S2A). KHK-C is mainly expressed in hepatocytes and has a much higher kinase activity in phosphorylating fructose to fructose-1-phosphate, while KHK-A participates in cancer progression in multipath[9,14,25]. The isoform analysis of the TCGA dataset indicated that the expression of KHK-A was far more than KHK-C in both colon and rectum cancer (Fig. 2E, Fig. S2B). The IHC of the previous mice's liver showed that KHK-A was remarkably expressed in liver metastatic tumors. In contrast, KHK-C was mainly expressed in hepatocytes (Fig. 2F). The results of qRT-PCR and WB with two isoforms' specific

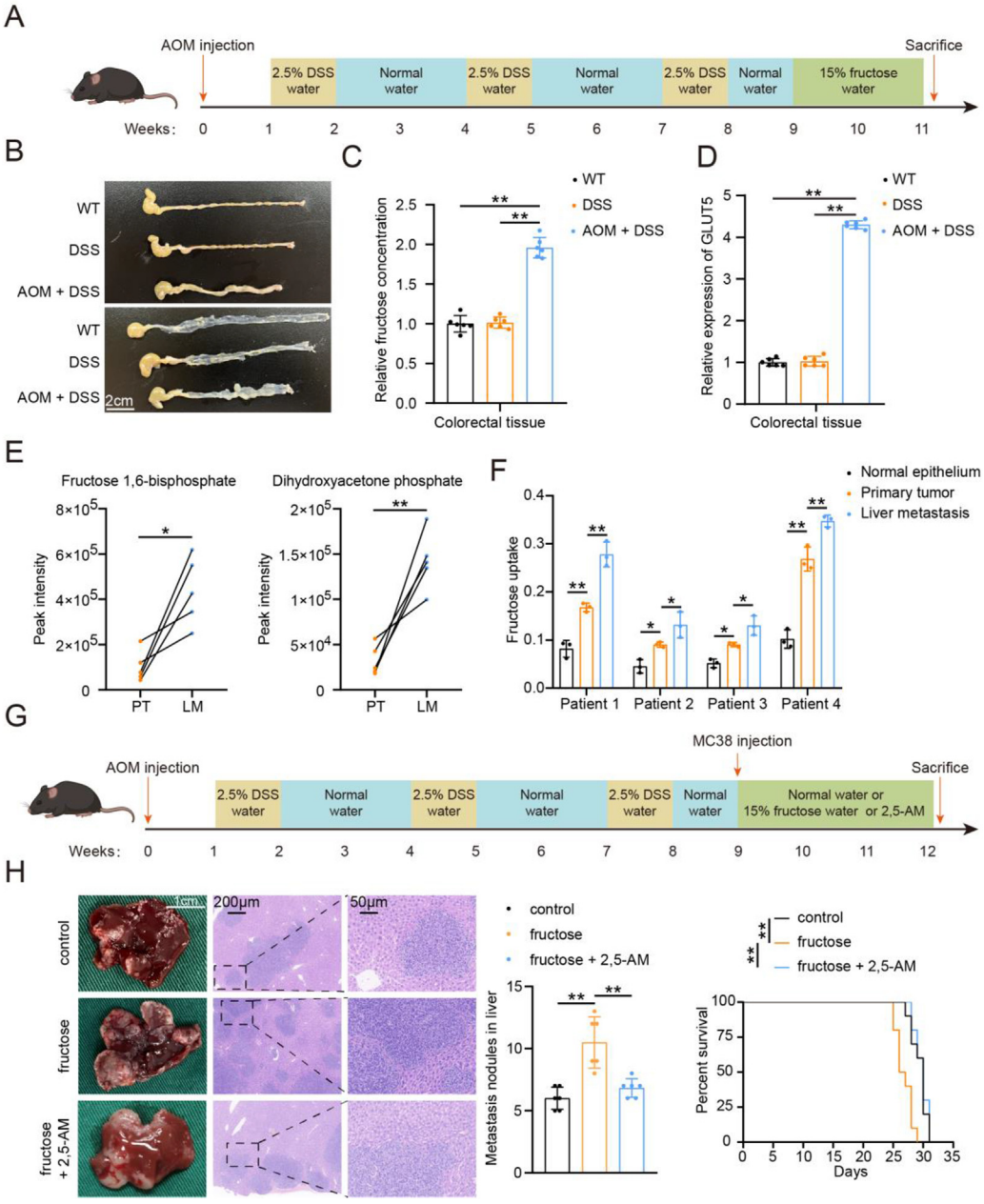

Figure 1 Fructose absorbed by colorectal cancer tissue could accelerate CRLM. (A) Schematic diagram of AOM/DSS model. (B) Representative images of mice colorectums. (C) Relative fructose concentration of mice colorectum tissues under fructose diet. (D) The mRNA expression of GLUT5 in relative mice colorectum tissues. (E) Relative peak intensity of fructose 1,6-bisphosphate and dihydroxyacetone phosphate in primary tumor (PT) and liver metastases (LM). (F) Fructose uptake analysis between paired adjacent normal colorectal tissues, primary colorectal cancer tissues and liver metastases of CRLM patients. (G) Schematic diagram of AOM/DSS model followed by MC38 intrasplenic injection with or without 2,5-AM treatment. For the 2,5-AM treatment group, 2,5-AM was intraperitoneally injected into AOM/DSS model mice at 150 mg/kg/day. (H) Relative images of the liver and HE staining of liver metastases separated from the above mice groups ($n = 6$) (left). Overall survival after intrasplenic injection was shown ($n = 10$) (right). Data are present as mean ± SD; $^{*}P < 0.05$, $^{**}P < 0.01$.

primers and antibodies in the above samples showed that KHK-A was significantly upregulated in liver metastases compared to the primary tumors. In contrast, the expression of KHK-C was low in both samples and had no significant difference (Fig. 2G and H, Fig. S2C). Furthermore, the IHC analysis of a tissue microarray constructed from 48 CRLM patients with synchronous liver resection illustrated the H-score and positive area of KHK-A in liver metastases was strikingly higher than that of the primary tumors (Fig. 2I–L). KHK-C was hardly detectable in two kinds of tissues (Fig. S2D). Additionally, KHK-A appeared to have a slight increase in response to fructose treatment (Fig. S2E). These results demonstrated that KHK-A, but not KHK-C, was significantly upregulated in liver metastasis compared to primary colorectal cancer.

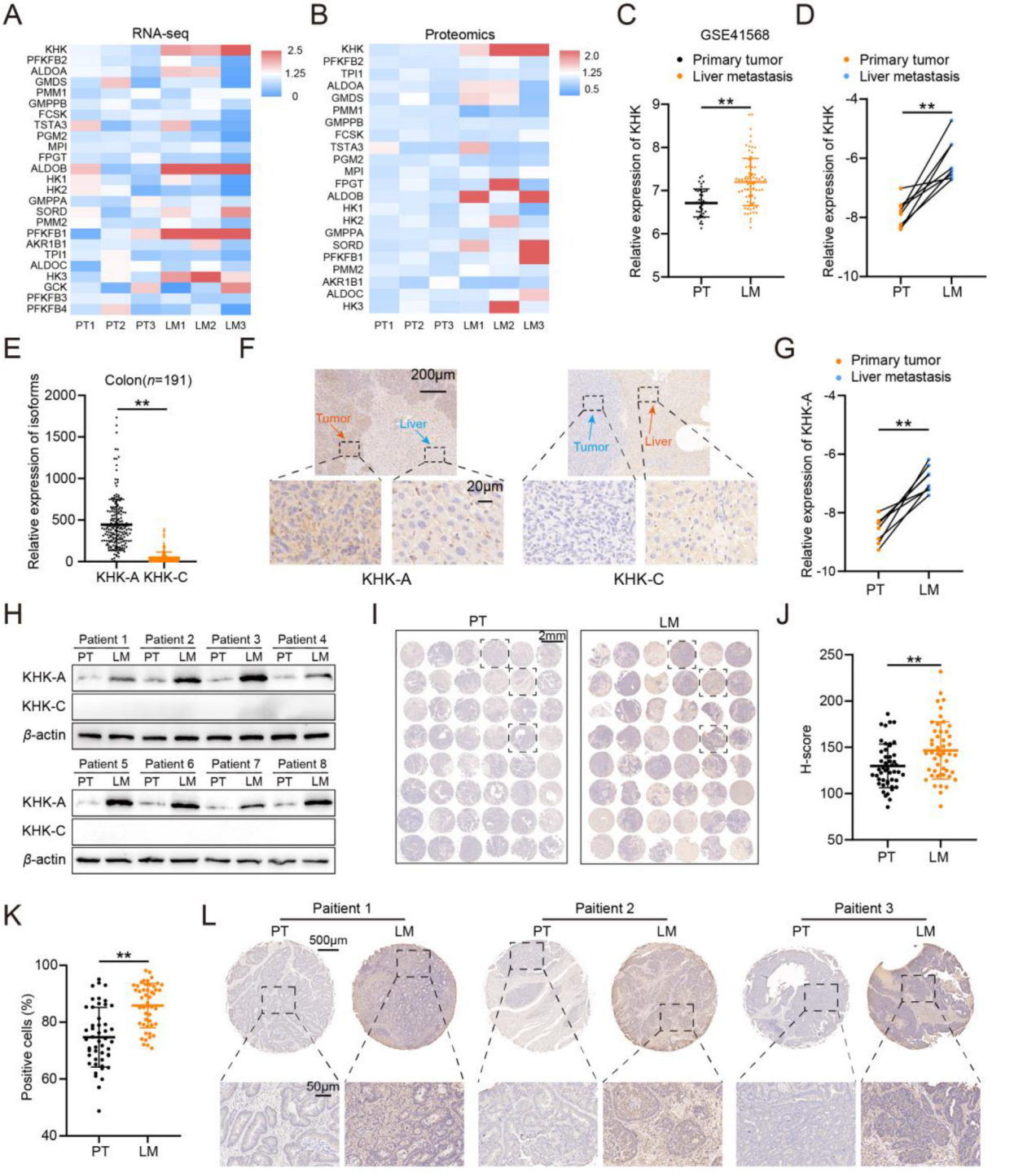

Figure 2 KHK-A, rather than KHK-C, was significantly upregulated in liver metastasis. (A–B) Relative expression of fructose metabolism enzyme (PubChem pathway: MI0035706) in RNA-seq (A) and proteomics (B) of paired primary tumors and liver metastases. (C) KHK expression in PT and LM according to GSE41568. (D) The expression of KHK in 8 paired PT and LM samples was detected by qRT-PCR. (E) The expression of two KHK isoforms in colon cancer according to TCGA. (F) IHC showed the expression of KHK-A and KHK-C in the normal liver and liver metastasis of CRLM mice in the control group of Fig. 1G. (G, H) KHK isoforms expression of 8 paired PT and LM samples. (I–L) A tissue microarray derived from CRLM patients after synchronous surgery was constructed to detect the expression of KHK-A. The H-score and positive cells of KHK-A in PT and LM tissue were quantified. Data are present as mean ± SD; $^{**}P < 0.01$.

3.3. KHK-A, rather than KHK-C, accelerated fructose-dependent CRLM in vitro and in vivo

To investigate the biological role of KHK-A in CRLM, we constructed DLD-1 and SW-480 cells with depleted endogenous KHK and reconstituted expression of KHK-A or KHK-C. The expression of KHK-A and KHK-C in relative cells was verified by qRT-PCR and WB (Supporting Information Fig. S3A and S3B). Migration assay in reconstituted KHK cells with or without 5 mmol/L fructose showed that KHK knockdown could attenuate fructose-induced cell migration and reconstituted KHK-A could strikingly restore the migration ability of DLD-1 and SW-480 cells, while the transmembrane cells of reconstituted KHK-C group appeared no significant than that of KHK knockdown group (Fig. 3A). Besides, KHK-A, rather than KHK-C, activated EMT (Fig. 3B, Fig. S3C). MC38 cells, which were transfected stably with sh-KHK and reconstituted KHK isoforms, were injected intrasplenically (Fig. S3D). Consistent with the observation *in vitro*, KHK-A overexpression, not KHK-C, accelerated fructose-induced CRLM. Besides, KHK knockdown could attenuate the metastatic effect of fructose (Fig. 3C and D). c-myc, a classic proto-oncogene in colorectal cancer progression, was upregulated by fructose diet and KHK-A overexpression (Fig. S3E)[26]. Recombinant KHK-A, rather than KHK-C, promoted tumor growth *in vivo* (Fig. S3F). In addition, 2,5-AM treatment could rescue the migration ability of DLD-1 and SW-480 cells with KHK-A overexpression, suggesting that intracellular fructose is indispensable for the upregulation of migration ability induced by KHK-A (Fig. S3G). The CRLM mice model illustrated that KHK-A accelerated CRLM progression *via* a fructose-dependent avenue (Fig. 3E and F). Collectively, KHK-A could activate EMT and promote fructose-independent CRLM *in vitro* and *in vivo*.

3.4. KHK-A bound to PKM2 and IMA-5 in response to intracellular fructose stimulation

Given that KHK-A could promote fructose-dependent CRLM, and it could barely utilize fructose for metabolism due to its low ketohexokinase enzymatic activity, we reconstituted KHK-A expression in DLD-1 and SW-480 cells with or without fructose stimulation to further explore its specific mechanism in CRLM (Fig. 4A). Several metabolic kinases could function as protein kinase and phosphorylate protein substrates directly to regulate multiple biological processes, according to emerging reports[13,14,27]. We performed co-immunoprecipitation in the above cells, and silver staining showed that KHK-A could bind to several specific proteins at about 65 kDa under fructose stimulation (Fig. 4B). Mass spectrometry and Venn Diagram showed that KHK-A could bind to PKM and IMA-5 (Importin subunit alpha-5) specifically upon fructose stimulation (Fig. 4C and Supporting Information Fig. S4A and S4B). We next verify that reconstituted KHK-A, not KHK-C, could bind to IMA-5 and PKM2, not PKM1 (Fig. 4D). PKM2 is a rate-limiting enzyme of glycolysis, and its phosphorylation modification has been reported to participate in various biological processes, including colorectal cancer progression[28-30]. A previous study reported that IMA-5 could transfer phosphorylated PKM2 to the cell nucleus and promote the Warburg effect, indicating that KHK-A might be involved in the phosphorylation and translocation of PKM2 by IMA-5[17]. Next, we constructed Co-IP in DLD-1 and SW-480 transfected with Flag-KHK-A or His-PKM2 with fructose stimulation. Exogenous KHK-A and PKM2 could bind with IMA-5 (Fig. S4C). Furthermore, Co-IP showed that endogenous KHK, PKM2 and IMA-5 could form ternary complex under fructose stimulation, and fructose could promote the interaction between PKM2 and IMA-5 (Fig. 4E). IF showed that KHK and PKM2 co-localized in DLD-1 and SW-480 (Fig. 4F). To further investigate the binding motif that accounted for PKM2 interacting with KHK-A, we transfected His-PKM2 or truncated mutations in DLD-1, followed by immunoprecipitation with His and immunoblot with KHK-A. The results showed that the C-domain of PKM2 was essential for its interaction with KHK-A (Fig. 4G). Given that KHK-A, not KHK-C, could bind to PKM2 and KHK-A had 45 amino acids different from KHK-C, we mutated the hydrophobic surface residues among them to verify the binding site for KHK-A binding to PKM2. Only the mutation of L73 could abolish the interaction between KHK-A and PKM2 (Fig. 4H). In addition, KHK-A could enhance the interaction of PKM2 and IMA-5, but KHK-A L73A and KHK-C could not (Fig. 4I). Furthermore, fructose uptake inhibition by 2,5-AM could impair the interaction between KHK-A and PKM2 or IMA-5 (Fig. S4D). Taken together, KHK-A could strengthen the PKM2/IMA-5 complex by direct binding, and the L73 residue of KHK-A was pivotal for the interaction with the C-domain of PKM2 upon fructose treatment.

3.5. PKM2 S37 phosphorylation facilitated by KHK-A inhibited the tetramer formation and pyruvic acid kinase activity of PKM2

PKM2 S37 phosphorylation could promote its *cis*−*trans* isomerization and bind to IMA-5 in brain tumorigenesis, indicating that KHK-A might participate in PKM2 S37 phosphorylation in CRLM[17]. The ATP-phosphate binding motif (GAGD) is indispensable for the kinase activity of KHK, and converting G257 residue to R can eliminate the kinase activity[14,31]. We constructed purified recombinant KHK-A wild-type, KHK-A L73A, KHK-A G257R, along with PKM2 wild-type, PKM2 S37D (Fig. 5A). GST pull-down under fructose stimulation demonstrated that KHK-A and KHK-A G257R, not KHK-A L73A, could directly bind to PKM2 (Fig. 5B). *In vitro* kinase assay elucidated that KHK-A WT, not KHK-A L73A or KHK-A G257R, could phosphorylate PKM2 at S37 but not PKM2 S37D (Fig. 5C). In line with this finding, KHK knockdown could decrease PKM2 S37 phosphorylation and recombinant expression of KHK-A WT, not KHK-A L73A or KHK-A G257R, could enhance PKM2 S37 phosphorylation under fructose stimulation (Fig. 5D). KHK-A overexpression significantly promoted PKM2 S37 phosphorylation in the above mice model (Supporting Information Fig. S5A and S5B). WB showed fructose uptake blocking inhibited PKM2 S37 phosphorylation induced by KHK-A (Fig. 5E). Similar results were presented in the mice model (Fig. 5F and Fig. S5C). The tetramer state of PKM2 has high pyruvic acid kinase (PK) activity, while the dimer or monomer state has low PK activity[32]. Phosphorylation of PKM2, including S37, could decrease the tetramer/dimer ratio and PK activity[30]. The BN-PAGE analysis showed that sh-KHK promoted the tetramer formation of PKM2. In contrast, recombinant KHK-A could dimerize PKM2, while recombinant KHK-A L73A and G257R did not alter the tetramer/dimer ratio with fructose culture (Fig. 5G). Similar results were detected in the PK activity assay (Fig. 5H). In addition, KHK-A L73A and G257R mutation dissociated PKM2 and IMA-5 compared to KHK-A WT, which indicated that KHK-A regulated the interaction between PKM2 and IMA-5 through binding to PKM2 and enhancing PKM2 S37 phosphorylation under

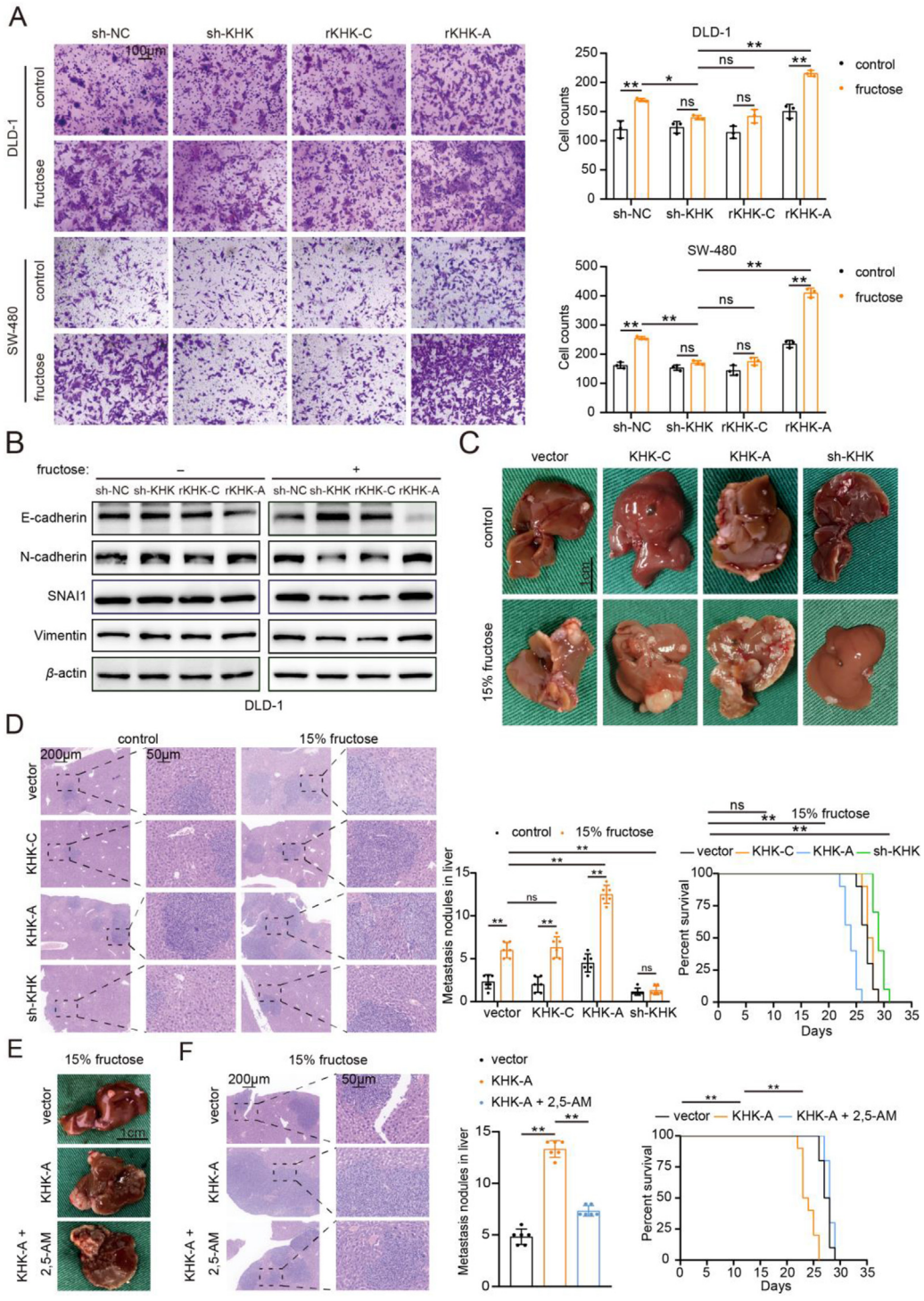

Figure 3 KHK-A, rather than KHK-C, accelerated fructose-dependent CRLM *in vitro* and *in vivo*. (A) Transwell assay detected the invasion ability of KHK knockdown and reconstituted KHK cells with or without fructose treatment. (B) The expression of EMT-related genes in relative groups. (C, D) MC38 cells with relative transfection were intrasplenically injected to construct the CRLM model with or without 15% fructose drinking water. The liver images and HE staining of liver metastases were shown ($n = 6$). Kaplan−Meier plots of mice survival were measured ($n = 10$). (E, F) The CRLM model was constructed as mentioned above, and 2,5-AM group mice were constructed by 2,5-AM intraperitoneal injection (150 mg/kg/day) ($n = 6$). Kaplan−Meier plots of mice survival were shown ($n = 10$). Data are present as mean ± SD; $^{*}P < 0.05$, $^{**}P < 0.01$. ns. not significant.

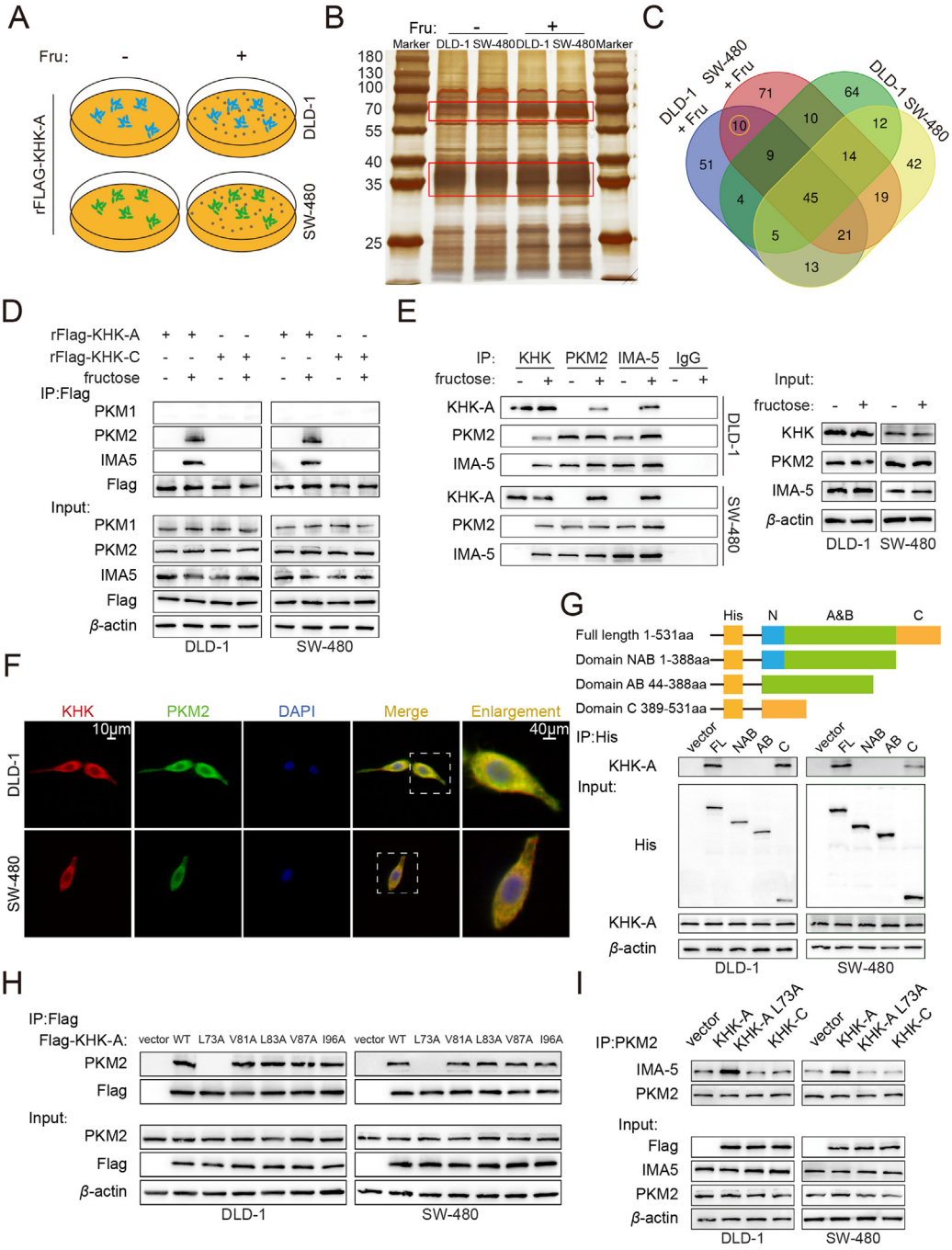

Figure 4 KHK-A bound to PKM2 and IMA-5 in response to intracellular fructose stimulation. (A) Schematic diagram of Co-IP. Co-IP was constructed in DLD-1 and SW-480 cells with recombinant KHK-A with or without fructose treatment. (B, C) Silver staining and mass spectrum of relative immunoprecipitation lysates. (D) The Co-IP assay was constructed in recombinant KHK-A/C cells with or without fructose treatment. (E) Co-IP assay was performed in wild-type DLD-1 and SW-480 cells with KHK, PKM2 and IMA-5 antibodies in the presence or absence of fructose treatment to explore the interaction among KHK-A, PKM2 and IMA-5. (F) KHK and PKM2 were co-localized in DLD-1 and SW-480 cells detected by IF with fructose treatment. (G) Fructose-treated DLD-1 and SW-480 cells were transfected with the indicated His-tagged PKM2 full length, along with its deletion mutants. The interaction between KHK-A and PKM2 was determined by Co-IP and immunoblotting. (H) Fructose-treated DLD-1 and SW-480 were transfected with KHK-A specific hydrophobic surface residues mutants, and Co-IP with anti-Flag antibody was performed. (I) Co-IP between IMA-5 and PKM2 in KHK-A, KHK-A L73A, and KHK-C overexpression cells with fructose treatment.

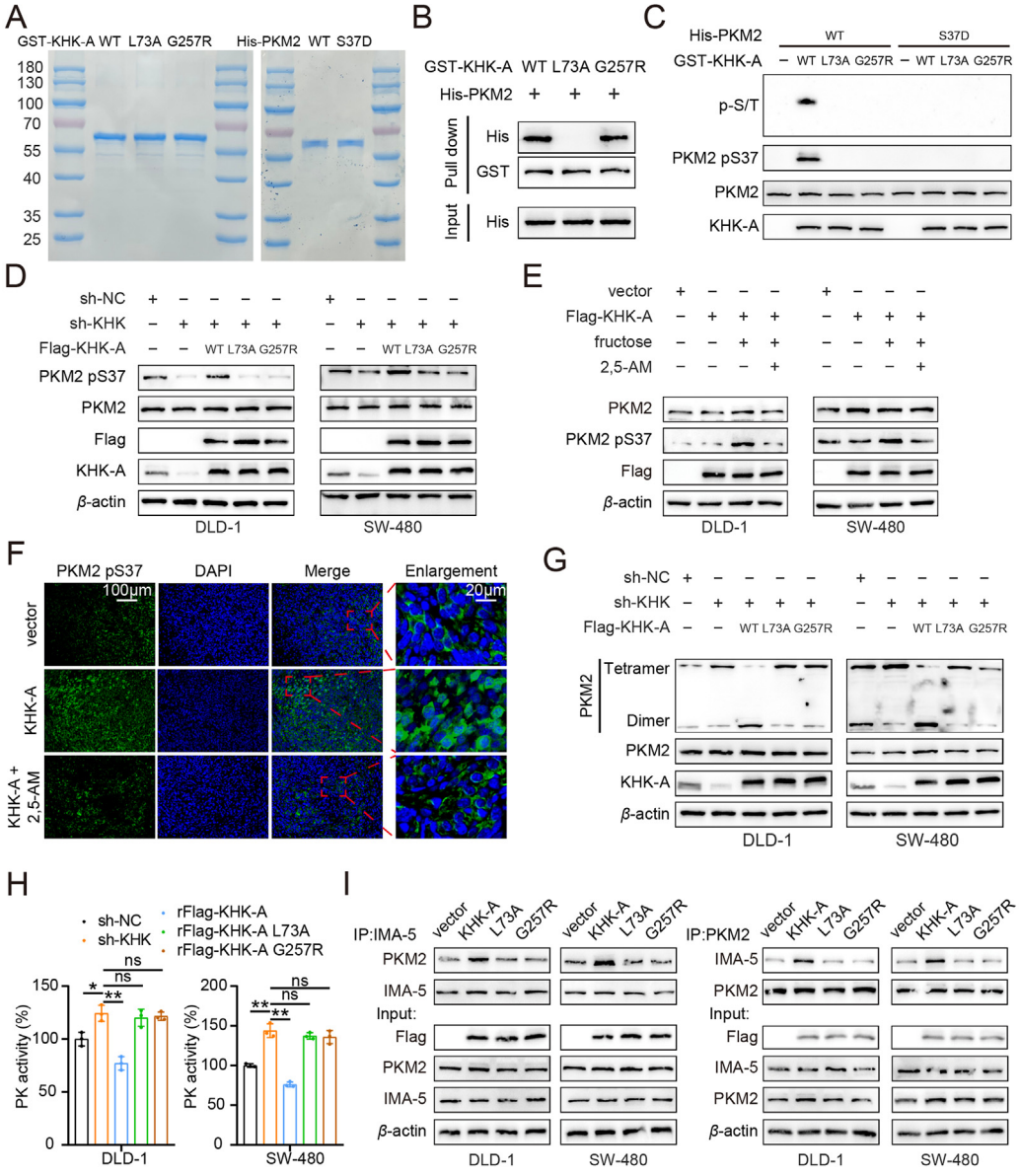

Figure 5 PKM2 S37 phosphorylation facilitated by KHK-A inhibited the tetramer formation and pyruvic acid kinase activity of PKM2. (A) Purified recombinant KHK-A wild-type, KHK-A L73A, KHK-A G257R, along with PKM2 wild-type, PKM2 S37D were constructed. (B) GST-pulldown was performed to explore the interaction between KHK-A and PKM2 with fructose treatment. (C) *In vitro* kinase assay between KHK-A and PKM2 with fructose treatment. (D) The phosphorylation of PKM2 at Ser37 was measured by WB in relative fructose-treated cells. (E) The phosphorylation level of PKM2 was detected in the relative group. (F) IF with PKM2 pS37 antibody in the above CRLM mice model. (G) BN-PAGE was performed to analyze PKM2 dimer and tetramer formation, and total PKM2 was detected by immunoblotting in fructose treatment cells. (H) PK activity was measured in relative cells with fructose treatment using the Pyruvate Kinase Activity Assay Kit. (I) Co-IP between IMA-5 and PKM2 in KHK-A, KHK-A L73A, and KHK-A G257R overexpression cells with fructose treatment. Data are present as mean ± SD; $^{*}P < 0.05$, $^{**}P < 0.01$. ns. not significant.

fructose stimulation (Fig. 5I). Collectively, these results showed that the interaction between KHK-A and PKM2 induced by fructose could promote PKM2 S37 phosphorylation.

3.6. KHK-A facilitated the Warburg effect by accelerating the IMA-5-induced nuclear translocation of PKM2

Given that IMA-5 could act as a nuclear transporter of PKM2 and KHK-A could enhance the interaction between PKM2 and IMA-5, we hypothesized that KHK-A could facilitate the nuclear accumulation of PKM2 induced by IMA-5. The subcellular protein fractions assay and IF indicated that the overexpression of KHK-A, not KHK-A L73A or G257R, promoted the translocation of PKM2 to the nucleus upon fructose treatment (Fig. 6A, Supporting Information Fig. S6A). Furthermore, depletion of IMA-5 inhibited KHK-A-induced nuclear accumulation of PKM2 under fructose stimulation (Fig. 6B, Fig. S6B). In line with these findings, exogenous KHK-A increased the nuclear fraction of His-

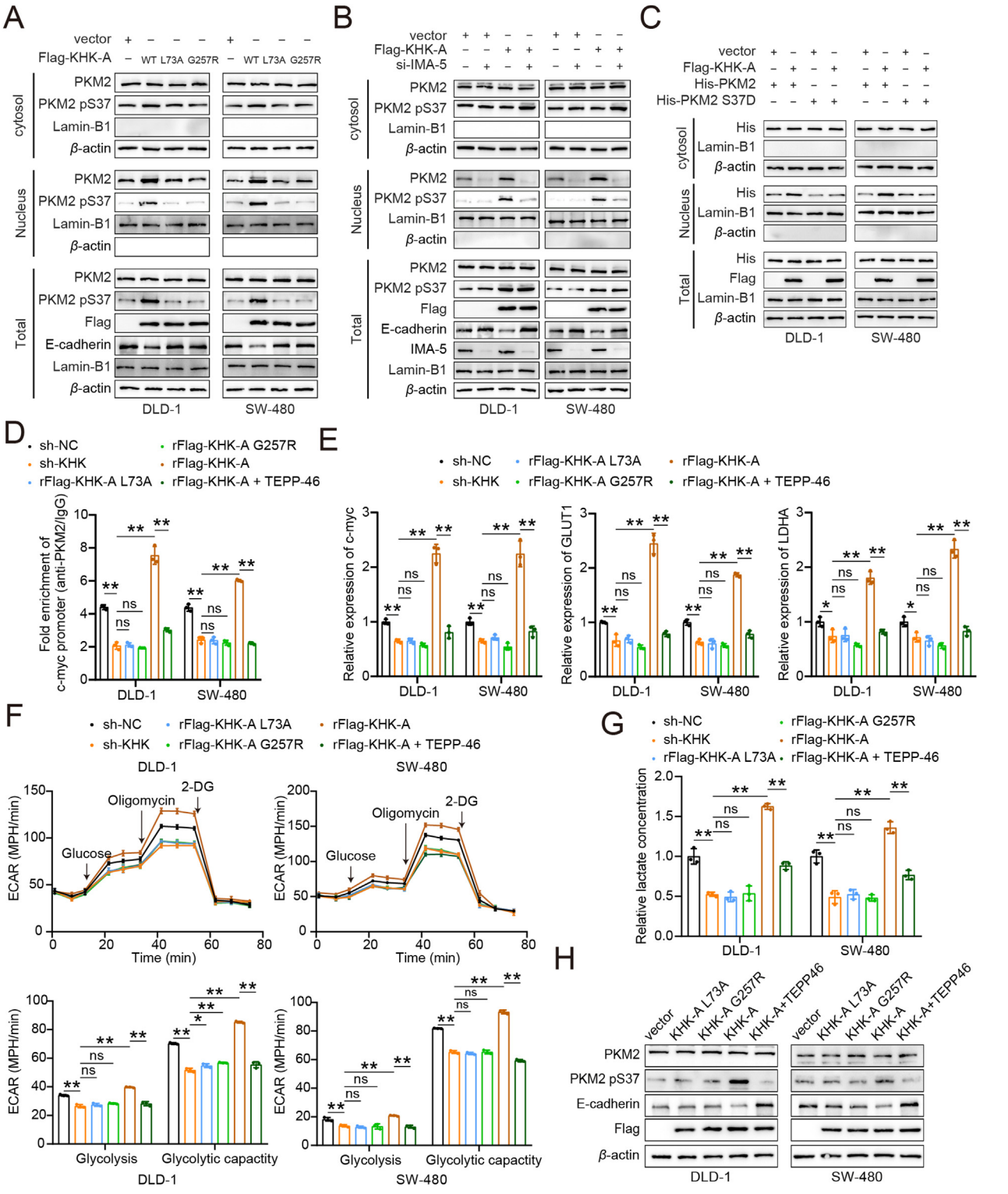

Figure 6 KHK-A facilitated the Warburg effect by accelerating the IMA-5-induced nuclear translocation of PKM2. (A–C) The subcellular protein fractions assays were performed in relative transfected cells. (D) ChIP assay to detect the enrichment of nuclear PKM2 at c-myc promoter (TEPP-46: 10 μmol/L for 24 h). (E) The expression of LDHA, GLUT1 and c-myc in relative cells was detected by qRT-PCR. (F) ECAR in the recombinant KHK-A groups, along with TEPP-46 treatment. (G) The concentration of lactate in the relative groups was detected by the Lactate Assay Kit. (H) E-cadherin expression was measured by WB. All cells involved in this figure were treated with 5 mmol/L fructose. Data are present as mean ± SD; $*P < 0.05$, $**P < 0.01$. ns. not significant.

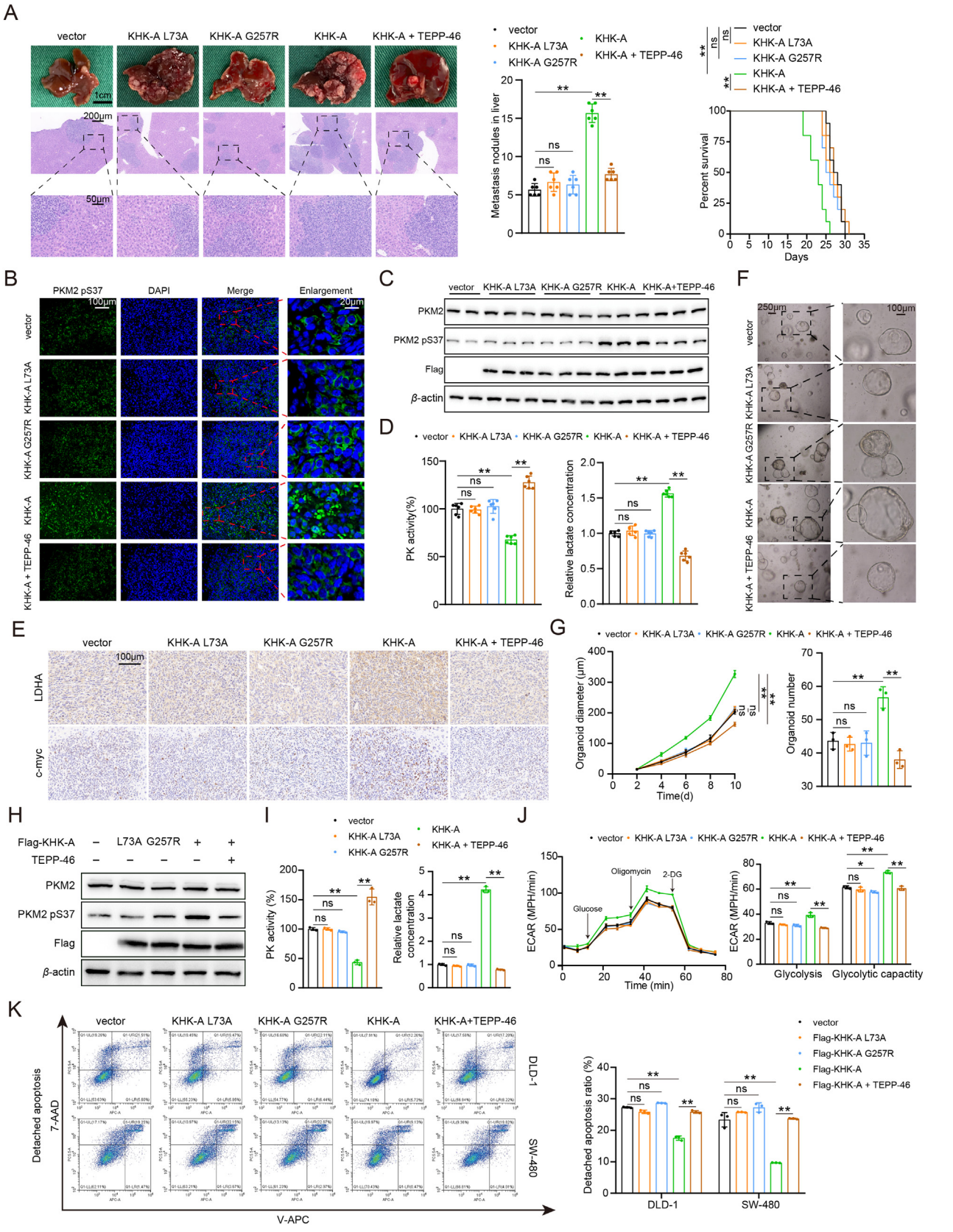

Figure 7 TEPP-46 could abolish KHK-A-induced CRLM with fructose treatment *in vitro* and *in vivo*. (A) MC38 cells with relative transfection were intrasplenically injected to construct the CRLM model with fructose drinking water. TEPP-46 was intraperitoneally injected (40 mg/kg) ($n = 6$) (left). Overall survival after intrasplenic injection was shown ($n = 10$) (right). (B, C) IF and WB were performed to detect PKM2 pS37 in the liver metastases of the CRLM mice model. (D) Relative PK activity and lactate concentration were detected in separated metastatic tumors.

PKM2, not His-PKM2 S37D, indicating that KHK-A promoted the IMA-5-dependent translocation of PKM2 through phosphorylating PKM2 at S37 residue (Fig. 6C). TEPP-46, a PK activator, could increase the PK activity of PKM2, dimeric PKM2 from tetramer formation, and inhibit S37 phosphorylation and nuclear accumulation of PKM2[30,33]. TEPP-46 could abolish KHK-A-induced S37 phosphorylation and nuclear accumulation of PKM2 in DLD-1 and SW-480 (Fig. S6C). TEPP-46 could also effectively upregulate PK activity in CRC (Fig. S6D). Therefore, TEPP-46 was applied to block PKM2 S37 phosphorylation in follow-up experiments.

It was reported that nuclear PKM2 could promote tumorigenesis-specific gene transcription, including c-myc-regulated genes such as GLUT1 and LDHA[13]. As mentioned above, c-myc was upregulated by KHK-A overexpression in a fructose-dependent way. Moreover, the ChIP assay with anti-PKM2 showed that KHK-A enhanced the transcription of c-myc *via* the nuclear PKM2 (Fig. 6D). c-myc, GLUT1 and LDHA was upregulated by recombinant KHK-A, not KHK-A L73A or G257R, and TEPP-46 could block the upregulation under fructose stimulation (Fig. 6E). In addition, ECAR in the recombinant KHK-A group significantly increased compared to the KHK-A mutant group and inhibition of PKM2 phosphorylation could impair ECAR under fructose stimulation (Fig. 6F). The lactate concentration decreased in KHK-depleted cells, and recombinant KHK-A, not KHK-A L73A or G257R, significantly increased lactate concentration, which could be abolished by TEEP-46 (Fig. 6G). Besides, nuclear PKM2 could promote histone deacetylation (H3K9) of the E-cadherin promoter to activate EMT in colorectal cancer[34]. The results of WB and qRT-PCR showed KHK-A inhibited E-cadherin expression through phosphorylation and translocation of PKM2 under fructose treatment (Fig. 6H and Fig. S6E). Furthermore, the ChIP assay performed with PKM2 and H3K9ac antibodies elucidated that KHK-A inhibited E-cadherin transcription by nuclear PKM2 and histone deacetylation under fructose stimulation (Fig. S6F and S6G). Taken together, KHK-A could facilitate aerobic glycolysis and EMT by accelerating IMA-5-induced nuclear translocation of PKM2 with fructose treatment.

3.7. *TEPP-46 abolished KHK-A-induced CRLM with fructose treatment in vitro and in vivo*

Next, we explored whether KHK-A accelerated fructose-dependent CRLM through phosphorylation PKM2 at S37. Transwell assay showed that KHK-A L73A and G257R failed to enhance the migration ability of CRC cells, and TEPP-46 treatment could attenuate the metastatic capacity of KHK-A overexpression cells under fructose stimulation (Supporting Information Fig. S7A). In line with these results, the CRLM mice model demonstrated that KHK-A mutations and TEPP-46 treatment could impair the liver metastasis accelerated by KHK-A with a high fructose diet. Similarly, KHK-A overexpression decreased the mice's survival, which was prolonged by TEPP-46 treatment (Fig. 7A). KHK-A accelerated the expression level and nuclear accumulation of PKM2 S37 phosphorylation, while TEPP-46 treatment inhibited its nuclear translocation in liver metastases (Fig. 7B and C). Similarly, the PK activity and lactate concentration of liver metastases were in line with previous results *in vitro* (Fig. 7D). Moreover, KHK-A, not KHK-A L73A or G257R, promoted the Warburg effect-associated genes in liver metastases (Fig. 7E and Fig. S7B). PT and LM organoids were constructed from patients who underwent synchronous surgery (Fig. S7C). The expression of KHK-A and PKM2 S37 phosphorylation in LM organoids was higher than in PT organoids, and fructose treatment could facilitate the phosphorylation of PKM2 at S37 in both PT and LM organoids (Fig. S7D). KHK-A wild-type and mutant overexpression lentivirus were transfected into LM organoids (Fig. 7F). KHK-A, not its mutants, promoted LM organoid growth, and TEPP-46 could inhibit the diameter and number of organoids (Fig. 7G). S37 phosphorylation of PKM2 and Warburg-associated genes increased in response to KHK-A overexpression in MT organoids (Fig. 7H and Fig. S7E). The PK activity of LM organoids significantly decreased in the KHK-A group, and TEPP-46 enhanced the PK activity of KHK-A overexpression organoids. The lactate concentration and ECAR were consistent with the results in cell lines (Fig. 7I and J). The Warburg effect can help metastatic cancer cells conquer heightened oxidative stress, facilitate anoikis resistance during detachment from the matrix and accelerate metastatic dissemination[35,36]. Accordingly, we planted CRC cells in ultra-low attached plates under fructose stimulation and detected the apoptosis ratio. KHK-A, not its mutations, promoted anoikis resistance of DLD-1 and SW-480 cells. In contrast, the TEPP-46 treatment decreased the detached apoptosis ratio of KHK-A overexpression cells (Fig. 7K). Taken together, KHK-A drives fructose-dependent CRLM by accelerating the S37 phosphorylation and translocation of PKM2.

3.8. *PKM2 S37 phosphorylation correlated with KHK-A expression of CRLM patients*

We analyze the expression of PKM2 S37 phosphorylation in paired primary tumors and liver metastases. PKM2 S37 phosphorylation, consistent with KHK-A, was significantly upregulated in liver metastases compared to primary tumors (Fig. 8A). S37 phosphorylated level of PKM2 was detected by IF in the tissue microarray (Fig. 8B and C). The mean density and positive area of PKM2 S37 phosphorylation in liver metastases were strikingly higher than in primary tumors (Fig. 8D and E). Furthermore, the H-score of KHK-A positively correlated with the positive area of PKM2 S37 phosphorylation in metastatic tumors (Fig. 8F). In addition, the transactivation gene of nuclear PKM2, including c-myc, GLUT1 and LDHA, was significantly upregulated in liver metastatic tumors (Fig. 8G−I). The expression of GLUT1 was significantly upregulated in liver metastases according to GSE41568 (Fig. 8J). The lactate concentration in liver metastasis was higher than in primary colorectal cancer (Fig. 8K). Furthermore, the metabolomics, as mentioned above, revealed a significantly increased abundance of glucose, reduced glutathione and ribose-5-phosphate in liver metastases compared to the

(E) IHC with LDHA and c-myc antibody was performed in the mice model. (F, G) LM organoids constructed from patients who underwent synchronous surgery were transfected with relative lentivirus. The LM organoid diameter and number were shown. (H, I) The PKM2 pS37 expression, PK activity and lactate concentration of LM organoids. (J) The ECAR of LM organoids was shown. (K) The apoptosis ratio of DLD-1 and SW-480 was detected by the Flow cytometry assay after being cultured in ultra-low attached plates with fructose treatment for 72 h. Data are present as mean ± SD; *$P < 0.05$, **$P < 0.01$. ns. not significant.

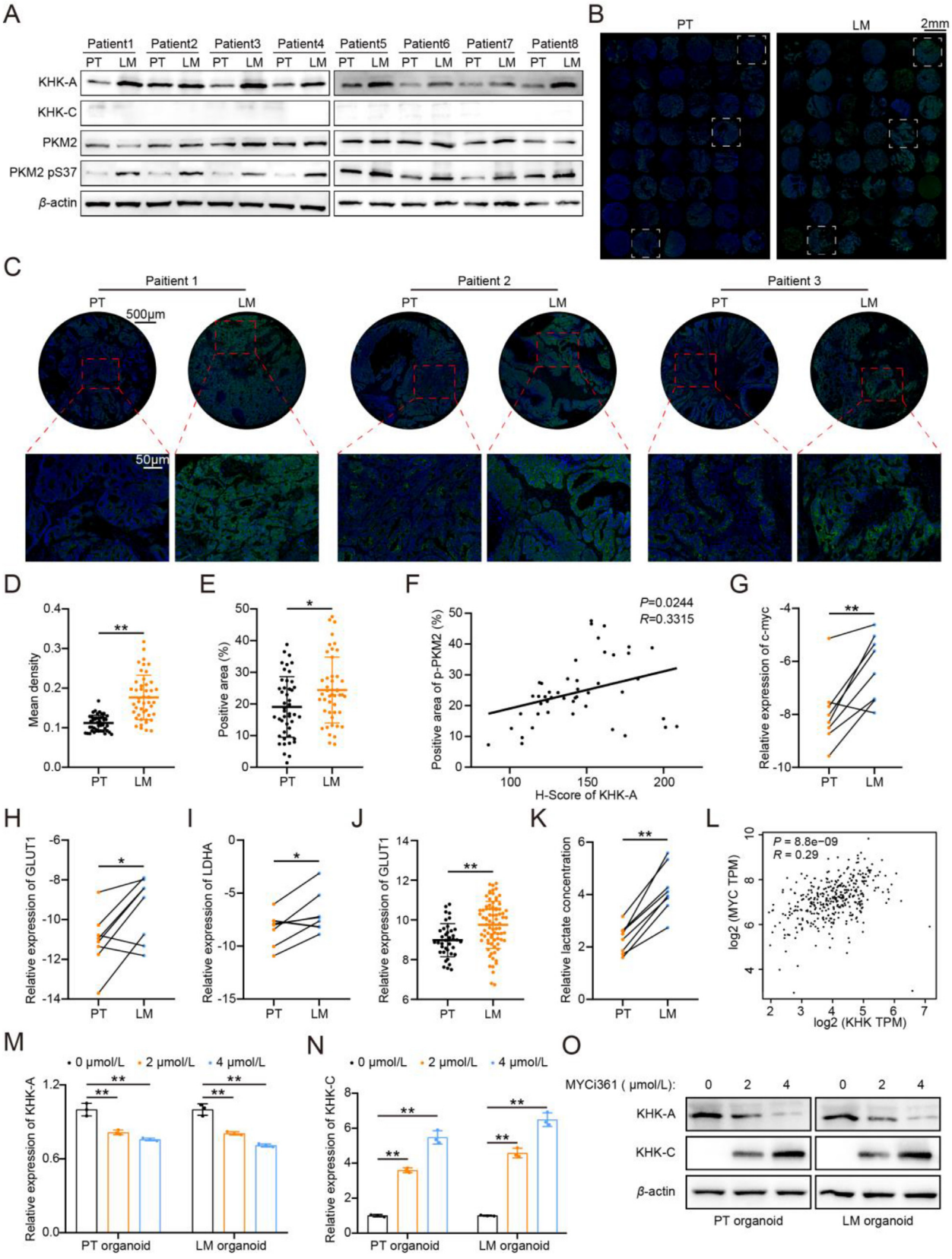

Figure 8 PKM2 S37 phosphorylation correlated with KHK-A expression of CRLM patients. (A) KHK and PKM2 pS37 expression in 8 paired PT and LM samples. (B−E) The expression of PKM2 pS37 in the tissue microarray detected by IF. (F) The correlation analysis between KHK-A and PKM2 pS37 according to the tissue microarray. (G−I) The mRNA expression of c-myc, GLUT1 and LDHA in 8 paired PT and LM tissues. (J) The expression of GLUT1 in PT and LM according to GSE41568. (K) The concentration of lactate in PT and LM was measured using the Lactate

primary tumors, which indicated that liver metastases presented a high aerobic glycolysis state (Supporting Information Fig. S8A−S8C). Notably, c-myc was essential for KHK-A isoform expression in hepatocellular carcinoma[14]. The expression of c-myc was positively correlated with KHK in colorectal cancer according to the TCGA dataset (Fig. 8L). The c-myc inhibitor (MYCi361) treatment resulted in a decrease in KHK-A expression, while KHK-C was upregulated by MYCi361 treatment in both PT and LM organoids (Fig. 8M−O). Similarly, the knockdown of c-myc in PT and LM organoids resulted in the alternative splicing transformation of KHK isoforms (Fig. S8D−S8E). In conclusion, these findings suggested that KHK-A and PKM2 S37 phosphorylation exhibited a concomitant upregulation. Aerobic glycolysis was activated in liver metastases compared to primary tumors. In turn, c-myc, upregulated by the nuclear PKM2, promoted the KHK-A isoform expression, forming a positive feedback loop in CRLM.

4. Discussion

CRLM is a multicausal and multistep pathological process[5]. The high fructose diet may play a vital role in CRLM, but its potential mechanism remains unclear[10]. The uptake ability of colorectal cancer tissues is higher than that of normal epithelial tissues, indicating that fructose absorbed by the primary tumor may accelerate CRLM. Notably, KHK-C is hardly expressed in colorectal cancer tissue, while KHK-A, with an ultra-low affinity for fructose phosphorylation, was significantly upregulated in metastases compared to primary tumors. This suggests that KHK-A and fructose may play an unknown role in CRLM. Here, we report that fructose absorbed by primary tumors facilitates the interaction between upregulated KHK-A and PKM2. KHK-A phosphorylates PKM2 at Ser37 directly and induces its nuclear accumulation, ultimately promoting EMT, aerobic glycolysis and CRLM.

Colorectal cancer liver metastasis is the leading cause of its high mortality. During the distant metastasis development of cancer, cancer cells must overcome physical and physiological stress[37]. Since approximately half of CRC patients have liver metastasis, cancer-distant metastasis itself exhibits a highly inefficient state[35,38]. Millions of cancer cells were migrating from primary tumor per gram mass daily, but only a few of the migrated cells could survive under harsh stress and actually form metastatic lesions, accounting for the circulating tumor cells' low metastatic predictive accuracy[35]. The metabolic switch helps detached cancer cells impair reactive oxygen species generation and promote anoikis resistance[39]. The Warburg metabolism is critical for metastasis formation[15]. According to the metabolomics dataset of CRLM, colorectal cancer liver metastasis exhibits a higher aerobic glycolysis state compared to the primary tumors, manifested by upregulated glucose, ribose-5-phosphate and reduced glutathione (Fig. S8A−S8C)[10,16]. PKM2 is considered the most significant regulator of the Warburg effect[32]. Its phosphorylation at Ser37 is identified as a potential prognostic indicator and therapeutic target in breast cancer[30]. Phosphorylation of PKM2 at Ser37 promotes the Warburg effect by increasing the dimer/tetramer ratio, accelerating the nuclear accumulation and decreasing the PK activity of PKM2[17,30]. The S37 phosphorylation of PKM2 is unregulated in liver metastases compared to primary cancer and correlates with KHK-A, indicating that KHK-A promotes CRLM by promoting the phosphorylation of PKM2 and Warburg metabolism.

The high fructose diet is widespread nowadays and a significant risk factor for CRC[5]. High dietary fructose facilitates CRC's proliferation and chemotherapy resistance *via* enhancing GLUT5−KHK interaction[11]. Physiological fructose transport is mediated by GLUT5 in small intestine epithelial cells[40]. However, the consumption of as little as 5 g of fructose caused the saturation of GLUT5 in the small intestine, resulting in an increased concentration of fructose in the lumen of the colon of humans[41-43]. Specifically, the fructose concentration was significantly increased in the colonic lumen (4.4 mmol/L at peak) in mice treated with high-fructose corn syrup[44]. So, we chose 5 mmol/L fructose for *in vitro* stimulation on colorectal cancer cells to mimic the effect of a high fructose diet on colorectal cancer cells. The liver microenvironment causes increased fructose metabolism of CRC cells during liver colonization by ALDOB[10]. ALDOB is also a key enzyme in fructose metabolism, which converts fructose-1-phosphate into glyceraldehyde and dihydroxyacetone phosphate and is upregulated after colorectal cancer cells colonize in the liver and accelerate cancer cell proliferation in livers. KHK and ALDOB in different stages of CRLM may possess potential synergies, as they do in fructose metabolism. Since the metabolic mechanism of fructose is distinguished from glucose, fructose facilitates glucose utilization and the Warburg effect[45]. This study may provide a feasible explanation for it in CRLM based on the low expression of KHK-C and high fructose uptake in CRC cells.

This study still has some limitations. KHK-A promotes fructose-dependent Ser37 phosphorylation of PKM2. L73 of KHK-A is essential for the binding, and G257 of KHK-A is indispensable for its kinase activity. Fructose is essential in this process. However, the precise role of fructose in this interaction remains to be explored. Similarly, fructose facilitates the formation of KHK-A, LRRC59 and KPNB1 complex in breast cancer. KHK-A can translocate to the nucleus upon fructose stimulation in breast cancer cells[9]. The role of fructose in these interactions may be similar and needs further exploration. A mouse model with both primary and liver metastatic tumors is indispensable in this study. However, the frequency of liver metastases is extremely low in the AOM/DSS model[24,46]. So, we injected CRC cells intrasplenically into the AOM/DSS model to mimic human CRLM progression as previously reported[21]. The AOM/DSS-related studies were mainly performed on C57BL/6, C57BL/6J, C57BL/6N and BALB/c[46]. So, we injected MC38 cells into the AOM/DSS mice to construct the CRLM model on C57BL/6J. Besides, several inhibitors were used to impair CRLM through metabolic and nonmetabolic paths. Among them, 2,5-AM is targeted on fructose uptake, and TEPP-46 inhibited phosphorylation and translocation of PKM2, while MYCi361 decreased the alternative splicing of KHK-A by targeting c-myc. Nevertheless, the combined application of inhibitors as target therapy of CRLM needs more experimental animal data and clinical-related trials.

In summary, we report that the fructose absorption ability of colorectal cancer tissues is higher than that of normal epithelial tissues. Fructose absorbed by colorectal cancer tissues is applied to generate liver metastases, and 2,5-AM impairs the CRLM accelerated by fructose. KHK-A, among the fructose metabolism

Assay Kit. (L) The correlation analysis between MYC and KHK according to GEPIA (http://gepia.cancer-pku.cn/). (M−O) The expression of KHK-A and KHK-C in PT and LM organoids in response to the MYCi361 treatment. Data are present as mean ± SD; *$P < 0.05$, **$P < 0.01$.

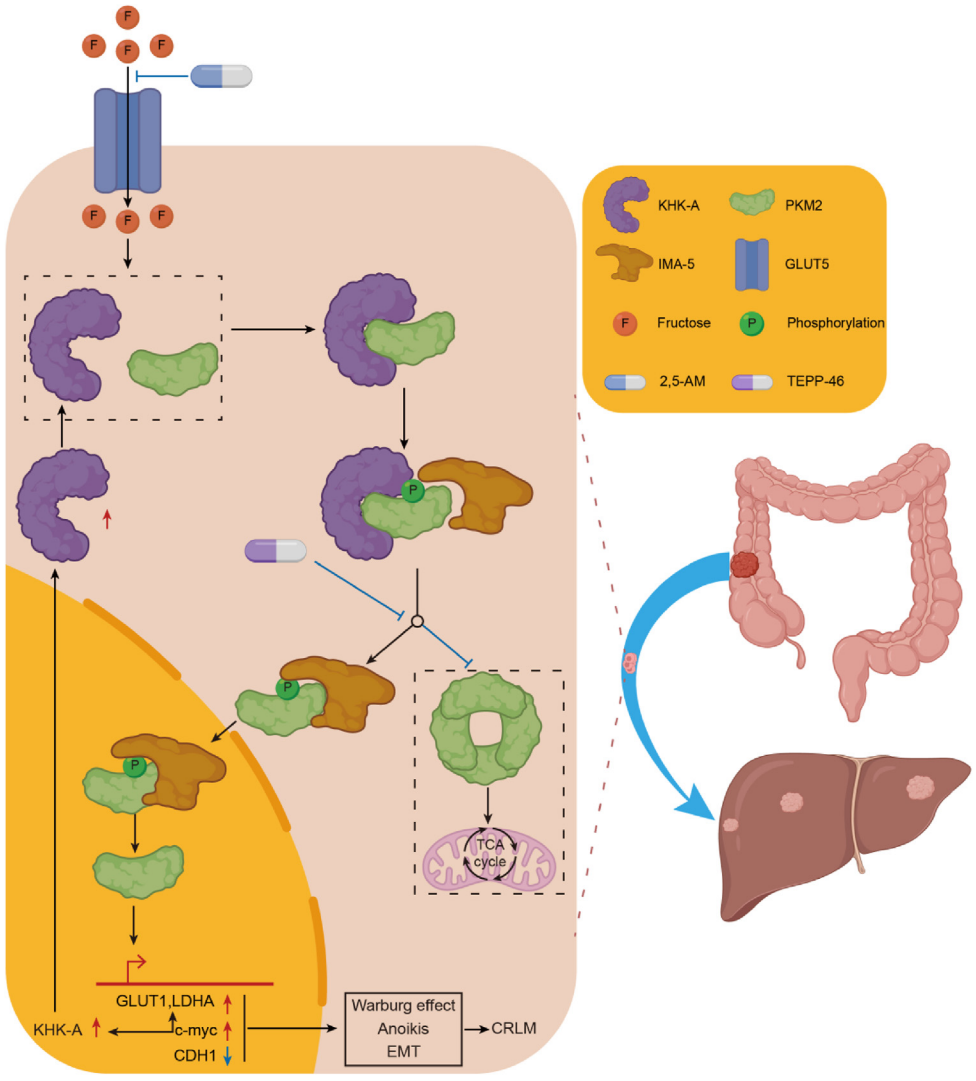

Figure 9 A Schematic diagram of this study. Upregulated KHK-A promoted fructose-dependent CRLM. KHK-A promoted the phosphorylation of PKM2 at Ser37 and the translocation of PKM2 to the nucleus. Meanwhile, the tetramer formation of PKM2 and the tricarboxylic acid cycle was inhibited by KHK-A. Nuclear PKM2 promoted EMT, aerobic glycolysis, CRLM, and alternative splicing of KHK-A.

enzymes, is upregulated in liver metastases compared to primary cancer and promotes fructose-dependent CRLM. KHK-A, not KHK-C, binds to PKM2 and IMA-5 in response to fructose stimulation. L73 of KHK-A and domain C of PKM2 are responsible for the binding. KHK-A facilitates CRLM by promoting the S37 phosphorylation and IMA-5-mediated nuclear accumulation of PKM2 pS37. Upregulated KHK-A promotes EMT and aerobic glycolysis *via* the above mechanism *in vitro* and *in vivo* (Fig. 9).

5. Conclusions

Fructose absorbed by colorectal cancer tissue is applied to generate liver metastasis. Upregulated KHK-A accelerates CRLM by binding to PKM2 and IMA-5. KHK-A facilitates CRLM by promoting the S37 phosphorylation and IMA-5-mediated nuclear accumulation of PKM2 pS37. Upregulated KHK-A promotes EMT and aerobic glycolysis *in vitro* and *in vivo*, which could be attenuated by TEEP-46. c-myc, which was upregulated by the nuclear PKM2, promoted the alternative splicing of KHK-A, forming a positive feedback loop in CRLM.

Acknowledgments

This study was funded by the National Natural Science Foundation (Grant Number 82273406), Basic Research Program of Jiangsu Province (Grant No. BK20201491, China), Nature Key Research and Development Program of Jiangsu Province (BE2021742, China), Jiangsu Province Capability Improvement Project through Science, Technology and Education (Jiangsu Provincial Medical Key Discipline, ZDXK202222, China), the National Natural Science Foundation (Grant Number 82203656, China). We want to thank the Core Facility of Jiangsu Provincial People's Hospital for its help in detecting experimental samples.

Author contributions

Yueming Sun and Chaofan Peng raised the hypothesis and designed the experiments. Chaofan Peng, Peng Yang, Dongsheng Zhang and Chi Jin performed experiments. Peng Yang performed animal experiments. Chaofan Peng, Wen Peng, Tuo Wang,

Qingyang Sun and Zhihao Chen analyzed the data. Yifei Feng drafted the manuscript. Yueming Sun supervised the research, secured funding, and interpreted the results. All authors read and approved the final manuscript.

Conflicts of interest

The authors declare that they have no known competing financial interests in this paper. The schematic illustration was created with Biorender.com.

Appendix A. Supporting information

Supporting information to this article can be found online at https://doi.org/10.1016/j.apsb.2024.04.024.

References

1. Siegel RL, Wagle NS, Cercek A, Smith RA, Jemal A. Colorectal cancer statistics, 2023. *CA Cancer J Clin* 2023;**73**:233−54.
2. Liu QL, Zhou H, Zhou ZG, Chen HN. Colorectal cancer liver metastasis: genomic evolution and crosstalk with the liver microenvironment. *Cancer Metastasis Rev* 2023;**42**:575−87.
3. Wang T, Sun F, Li C, Nan P, Song Y, Wan X, et al. MTA1, a novel ATP synthase complex modulator, enhances colon cancer liver metastasis by driving mitochondrial metabolism reprogramming. *Adv Sci (Weinh)* 2023;**10**:e2300756.
4. Tsilimigras DI, Brodt P, Clavien PA, Muschel RJ, D'Angelica MI, Endo I, et al. Liver metastases. *Nat Rev Dis Prim* 2021;**7**:27.
5. Hofseth LJ, Hebert JR, Chanda A, Chen H, Love BL, Pena MM, et al. Early-onset colorectal cancer: initial clues and current views. *Nat Rev Gastroenterol Hepatol* 2020;**17**:352−64.
6. Narayan RR, Aveson VG, Chou JF, Walch HS, Sanchez-Vega F, Santos Fernandes GD, et al. Association of genomic profiles and survival in early onset and screening-age colorectal cancer patients with liver metastases resected over 15 years. *J Surg Oncol* 2022;**125**:880−8.
7. Jiang H, Lin Q, Ma L, Luo S, Jiang X, Fang J, et al. Fructose and fructose kinase in cancer and other pathologies. *J Genet Genomics* 2021;**48**:531−9.
8. Liu H, Huang D, McArthur DL, Boros LG, Nissen N, Heaney AP. Fructose induces transketolase flux to promote pancreatic cancer growth. *Cancer Res* 2010;**70**:6368−76.
9. Kim J, Kang J, Kang YL, Woo J, Kim Y, Huh J, et al. Ketohexokinase-A acts as a nuclear protein kinase that mediates fructose-induced metastasis in breast cancer. *Nat Commun* 2020;**11**:5436.
10. Bu P, Chen KY, Xiang K, Johnson C, Crown SB, Rakhilin N, et al. Aldolase B-mediated fructose metabolism drives metabolic reprogramming of colon cancer liver metastasis. *Cell Metabol* 2018;**27**.1249-62.e4.
11. Shen Z, Li Z, Liu Y, Li Y, Feng X, Zhan Y, et al. GLUT5-KHK axis-mediated fructose metabolism drives proliferation and chemotherapy resistance of colorectal cancer. *Cancer Lett* 2022;**534**:215617.
12. Tong Y, Guo D, Lin SH, Liang J, Yang D, Ma C, et al. SUCLA2-coupled regulation of GLS succinylation and activity counteracts oxidative stress in tumor cells. *Mol Cell* 2021;**81**:2303-16.e8.
13. Lu Z, Hunter T. Metabolic kinases moonlighting as protein kinases. *Trends Biochem Sci* 2018;**43**:301−10.
14. Li X, Qian X, Peng LX, Jiang Y, Hawke DH, Zheng Y, et al. A splicing switch from ketohexokinase-C to ketohexokinase-A drives hepatocellular carcinoma formation. *Nat Cell Biol* 2016;**18**:561−71.
15. Lu J, Tan M, Cai Q. The Warburg effect in tumor progression: mitochondrial oxidative metabolism as an anti-metastasis mechanism. *Cancer Lett* 2015;**356**:156−64.
16. Nguyen A, Loo JM, Mital R, Weinberg EM, Man FY, Zeng Z, et al. PKLR promotes colorectal cancer liver colonization through induction of glutathione synthesis. *J Clin Invest* 2016;**126**:681−94.
17. Yang W, Zheng Y, Xia Y, Ji H, Chen X, Guo F, et al. ERK1/2-dependent phosphorylation and nuclear translocation of PKM2 promotes the Warburg effect. *Nat Cell Biol* 2012;**14**:1295−304.
18. Jin C, Wang T, Zhang D, Yang P, Zhang C, Peng W, et al. Acetyltransferase NAT10 regulates the Wnt/beta-catenin signaling pathway to promote colorectal cancer progression *via* ac^4C acetylation of KIF23 mRNA. *J Exp Clin Cancer Res* 2022;**41**:345.
19. Yang P, Li J, Peng C, Tan Y, Chen R, Peng W, et al. TCONS_00012883 promotes proliferation and metastasis *via* DDX3/YY1/MMP1/PI3K−AKT axis in colorectal cancer. *Clin Transl Med* 2020;**10**:e211.
20. Mo S, Tang P, Luo W, Zhang L, Li Y, Hu X, et al. Patient-derived organoids from colorectal cancer with paired liver metastasis reveal tumor heterogeneity and predict response to chemotherapy. *Adv Sci (Weinh)* 2022;**9**:e2204097.
21. Bertocchi A, Carloni S, Ravenda PS, Bertalot G, Spadoni I, Lo Cascio A, et al. Gut vascular barrier impairment leads to intestinal bacteria dissemination and colorectal cancer metastasis to liver. *Cancer Cell* 2021;**39**:708−724.e11.
22. Chen WL, Jin X, Wang M, Liu D, Luo Q, Tian H, et al. GLUT5-mediated fructose utilization drives lung cancer growth by stimulating fatty acid synthesis and AMPK/mTORC1 signaling. *JCI Insight* 2020;**5**:e131596.
23. Chen WL, Wang YY, Zhao A, Xia L, Xie G, Su M, et al. Enhanced fructose utilization mediated by SLC2A5 is a unique metabolic feature of acute myeloid leukemia with therapeutic potential. *Cancer Cell* 2016;**30**:779−91.
24. Rosenberg DW, Giardina C, Tanaka T. Mouse models for the study of colon carcinogenesis. *Carcinogenesis* 2008;**30**:183−96.
25. Xu D, Li X, Shao F, Lv G, Lv H, Lee JH, et al. The protein kinase activity of fructokinase A specifies the antioxidant responses of tumor cells by phosphorylating p62. *Sci Adv* 2019;**5**:eaav4570.
26. Loevenich LP, Tschurtschenthaler M, Rokavec M, Silva MG, Jesinghaus M, Kirchner T, et al. SMAD4 loss induces c-MYC-mediated NLE1 upregulation to support protein biosynthesis, colorectal cancer growth, and metastasis. *Cancer Res* 2022;**82**:4604−23.
27. Li X, Jiang Y, Meisenhelder J, Yang W, Hawke DH, Zheng Y, et al. Mitochondria-translocated PGK1 functions as a protein kinase to coordinate glycolysis and the TCA cycle in tumorigenesis. *Mol Cell* 2016;**61**:705−19.
28. Zhao G, Yuan H, Li Q, Zhang J, Guo Y, Feng T, et al. DDX39B drives colorectal cancer progression by promoting the stability and nuclear translocation of PKM2. *Signal Transduct Targeted Ther* 2022;**7**:275.
29. Chen Z, Wang Z, Guo W, Zhang Z, Zhao F, Zhao Y, et al. TRIM35 Interacts with pyruvate kinase isoform M2 to suppress the Warburg effect and tumorigenicity in hepatocellular carcinoma. *Oncogene* 2015;**34**:3946−56.
30. Apostolidi M, Vathiotis IA, Muthusamy V, Gaule P, Gassaway BM, Rimm DL, et al. Targeting pyruvate kinase M2 phosphorylation reverses aggressive cancer phenotypes. *Cancer Res* 2021;**81**:4346−59.
31. Trinh CH, Asipu A, Bonthron DT, Phillips SE. Structures of alternatively spliced isoforms of human ketohexokinase. *Acta Crystallogr D Biol Crystallogr* 2009;**65**:201−11.
32. Alquraishi M, Puckett DL, Alani DS, Humidat AS, Frankel VD, Donohoe DR, et al. Pyruvate kinase M2: a simple molecule with complex functions. *Free Radic Biol Med* 2019;**143**:176−92.
33. Anastasiou D, Yu Y, Israelsen WJ, Jiang JK, Boxer MB, Hong BS, et al. Pyruvate kinase M2 activators promote tetramer formation and suppress tumorigenesis. *Nat Chem Biol* 2012;**8**:839−47.
34. Hamabe A, Konno M, Tanuma N, Shima H, Tsunekuni K, Kawamoto K, et al. Role of pyruvate kinase M2 in transcriptional

regulation leading to epithelial-mesenchymal transition. *Proc Natl Acad Sci U S A* 2014;**111**:15526−31.
35. Lu J. The Warburg metabolism fuels tumor metastasis. *Cancer Metastasis Rev* 2019;**38**:157−64.
36. Wang YN, Zeng ZL, Lu J, Wang Y, Liu ZX, He MM, et al. CPT1A-mediated fatty acid oxidation promotes colorectal cancer cell metastasis by inhibiting anoikis. *Oncogene* 2018;**37**:6025−40.
37. Piskounova E, Agathocleous M, Murphy MM, Hu Z, Huddlestun SE, Zhao Z, et al. Oxidative stress inhibits distant metastasis by human melanoma cells. *Nature* 2015;**527**:186−91.
38. Zhong X, He X, Wang Y, Hu Z, Huang H, Zhao S, et al. Warburg effect in colorectal cancer: the emerging roles in tumor microenvironment and therapeutic implications. *J Hematol Oncol* 2022;**15**:160.
39. Kamarajugadda S, Stemboroski L, Cai Q, Simpson NE, Nayak S, Tan M, et al. Glucose oxidation modulates anoikis and tumor metastasis. *Mol Cell Biol* 2012;**32**:1893−907.
40. Drozdowski LA, Thomson AB. Intestinal sugar transport. *World J Gastroenterol* 2006;**12**:1657−70.
41. Rumessen JJ, Gudmand-Høyer E. Absorption capacity of fructose in healthy adults. Comparison with sucrose and its constituent monosaccharides. *Gut* 1986;**27**:1161−8.
42. Ravich WJ, Bayless TM, Thomas M. Fructose: incomplete intestinal absorption in humans. *Gastroenterology* 1983;**84**:26−9.
43. Beyer PL, Caviar EM, McCallum RW. Fructose intake at current levels in the United States may cause gastrointestinal distress in normal adults. *J Am Diet Assoc* 2005;**105**:1559−66.
44. Goncalves MD, Lu C, Tutnauer J, Hartman TE, Hwang SK, Murphy CJ, et al. High-fructose corn syrup enhances intestinal tumor growth in mice. *Science* 2019;**363**:1345−9.
45. Nakagawa T, Lanaspa MA, Millan IS, Fini M, Rivard CJ, Sanchez-Lozada LG, et al. Fructose contributes to the Warburg effect for cancer growth. *Cancer Metabol* 2020;**8**:16.
46. Dzhalilova D, Zolotova N, Fokichev N, Makarova O. Murine models of colorectal cancer: the azoxymethane (AOM)/dextran sulfate sodium (DSS) model of colitis-associated cancer. *PeerJ* 2023;**11**:e16159.